Clinical Cancer Research

SRRM4 Expression and the Loss of REST Activity May Promote the Emergence of the Neuroendocrine Phenotype in Castration-Resistant Prostate Cancer

Xiaotun Zhang[1], Ilsa M. Coleman[2], Lisha G. Brown[1], Lawrence D. True[3], Lori Kollath[1], Jared M. Lucas[2], Hung-Ming Lam[1], Ruth Dumpit[2], Eva Corey[1], Lisly Chéry[1], Bryce Lakely[1], Celestia S. Higano[1,4], Bruce Montgomery[4], Martine Roudier[1], Paul H. Lange[1,5], Peter S. Nelson[2,4], Robert L. Vessella[1,5], and Colm Morrissey[1]

Abstract

Purpose: The neuroendocrine phenotype is associated with the development of metastatic castration-resistant prostate cancer (CRPC). Our objective was to characterize the molecular features of the neuroendocrine phenotype in CRPC.

Experimental Design: Expression of chromogranin A (CHGA), synaptophysin (SYP), androgen receptor (AR), and prostate-specific antigen (PSA) was analyzed by IHC in 155 CRPC metastases from 50 patients and in 24 LuCaP prostate cancer patient-derived xenografts (PDX). Seventy-one of 155 metastases and the 24 LuCaP xenograft lines were analyzed by whole-genome microarrays. *REST* splicing was verified by PCR.

Results: Coexpression of CHGA and SYP in >30% of cells was observed in 22 of 155 metastases (9 patients); 11 of the 22 metastases were AR^+/PSA^+ (6 patients), 11/22 were AR–/PSA– (4 patients), and 4/24 LuCaP PDXs were AR^-/PSA^-. By IHC, of the 71 metastases analyzed by whole-genome microarrays, 5 metastases were $CHGA^+/SYP^+/AR^-$, and 5 were $CHGA^+/SYP^+/AR^+$. Only $CHGA^+/SYP^+$ metastases had a neuroendocrine transcript signature. The neuronal transcriptional regulator SRRM4 transcript was associated with the neuroendocrine signature in $CHGA^+/SYP^+$ metastases and all $CHGA^+/SYP^+$ LuCaP xenografts. In addition, expression of SRRM4 in LuCaP neuroendocrine xenografts correlated with a splice variant of *REST* that lacks the transcriptional repressor domain.

Conclusions: (i) Metastatic neuroendocrine status can be heterogeneous in the same patient, (ii) the CRPC neuroendocrine molecular phenotype can be defined by $CHGA^+/SYP^+$ dual positivity, (iii) the neuroendocrine phenotype is not necessarily associated with the loss of AR activity, and (iv) the splicing of *REST* by SRRM4 could promote the neuroendocrine phenotype in CRPC. *Clin Cancer Res; 21(20); 4698–708. ©2015 AACR.*

Introduction

It is widely believed that prostate neuroendocrine cells act in a secretory and autocrine/paracrine fashion that neuroendocrine cells of varying number are present in a significant proportion of primary prostate cancers, and, importantly, that neuroendocrine cells do not express the androgen receptor (AR; refs. 1, 2). The role that these neuroendocrine cells play in prostate cancer tumorigenesis is unknown, but appears to be gaining increasing importance in clinical progression after therapy with the new hormonal agents, enzalutamide, and abiraterone. Morphologically, some prostate cancer cells with neuroendocrine differentiation may eventually become malignant neuroendocrine cells (3), but others may remain similar to adenocarcinoma, and only methods targeting neuroendocrine markers can identify these cells (4). Although uncommon in primary prostate cancer, neuroendocrine tumors appear to be more prevalent in castration-resistant prostate cancer (CRPC; refs. 5–8).

Initially, prostate cancer is almost always hormone sensitive and responds to androgen deprivation therapy (ADT); however, the majority of patients eventually progress to CRPC. It has been hypothesized that the neuroendocrine differentiated population of cells in CRPC disease stimulate tumor growth and cell proliferation in an autocrine–paracrine fashion in an altered microenvironment with very low to no androgen levels (3, 9). It is further suggested that the newly acquired neuroendocrine phenotype in adenocarcinoma represents a mechanism through which hormone-sensitive prostate cancer develops resistance to ADT (10). Thus, the population of cells with neuroendocrine differentiation might be an important therapeutic target that could prevent the transformation of hormone-sensitive prostate cancer to CRPC. Currently, however, there is no effective treatment for

[1]Department of Urology, University of Washington, Seattle, Washington. [2]Divison of Human Biology, Fred Hutchinson Cancer Research Center, Seattle, Washington. [3]Department of Pathology, University of Washington, Seattle, Washington. [4]Department of Medicine, University of Washington, Seattle, Washington. [5]Department of Veterans Affairs Medical Center, Seattle, Washington.

Note: Supplementary data for this article are available at Clinical Cancer Research Online (http://clincancerres.aacrjournals.org/).

Corresponding Author: Colm Morrissey, University of Washington, 1959 NE Pacific Street, Seattle, WA 98195, Phone: 206-543-1461; Fax: 206-543-1146; E-mail: cmorriss@u.washington.edu

doi: 10.1158/1078-0432.CCR-15-0157

Translational Relevance

With the advent of total androgen blockade for the treatment of metastatic prostate cancer, there could be a significant increase in the number of patients with neuroendocrine disease. To treat patients with neuroendocrine disease, we need to understand the molecular basis for the emergence of neuroendocrine disease in castrate-resistant prostate cancer (CRPC) and identify targets associated with neuroendocrine disease. This study highlights (i) an increase in the neuroendocrine phenotype in CRPC relative to primary prostate cancer; (ii) that chromogranin A and synaptophysin-positive CRPC metastases can be androgen receptor (AR) positive and AR negative, representing different molecular phenotypes; and (iii) that patients can have metastases with neuroendocrine features and adenocarcinoma. Furthermore, our findings suggest that the evolution of adenocarcinoma from a hormone-sensitive state to a castration-resistant neuroendocrine phenotype is associated with the loss of REST or of REST-repressor activity due to alternate splicing by SRRM4.

prostate cancer with neuroendocrine differentiation. This is most likely due to our limited knowledge of the neuroendocrine phenotype in prostate cancer.

In this study, tissue markers [chromogranin A (CHGA)] and synaptophysin (SYP) for neuroendocrine differentiation, and AR were evaluated in conjunction with gene-expression profiling to determine the prevalence and molecular profile of the neuroendocrine phenotype in CRPC metastases and neuroendocrine LuCaP patient-derived xenografts (PDX). We determined that these three tissue markers are sufficient to identify CRPC metastases with a neuroendocrine molecular phenotype. On the basis of our findings, we speculate on the possible roles of serine/arginine–repetitive matrix 4 (SRRM4) and RE1-silencing transcription factor (REST) neural-specific regulators of transcription in the emergence of the neuroendocrine phenotype in CRPC (11, 12).

Materials and Methods

Reagents

The antibodies used in this study are listed in Supplementary Table S1.

Tissue acquisition

Samples were obtained from patients who died of metastatic CRPC and who signed written informed consent for a rapid autopsy performed within 6 hours of death, under the aegis of the Prostate Cancer Donor Program at the University of Washington (13). The Institutional Review Boards of the University of Washington and of the Fred Hutchinson Cancer Research Center approved this study. Visceral metastases were identified at the gross level, bone biopsies were obtained according to a template from 20 different sites and metastases identified at a histologic level. LuCaP xenograft lines were established from specimens acquired at either radical prostatectomy or at autopsy, implanted, and maintained by serial passage in intact immune compromised male mice (14).

Tissue microarray construction

One hundred and fifty-five prostate cancer metastases (including 73 visceral metastases and 82 bone metastases) from 50 autopsy patients (up to 4 sites per patient) were fixed in buffered formalin (bone metastases were decalcified in 10% formic acid) and embedded in paraffin. A tissue microarray (TMA) was made using duplicate 1-mm diameter cores from these tissues. A second TMA using duplicate 1-mm diameter cores from each of 24 LuCaP xenograft lines was also constructed.

RNA isolation

Total RNA was isolated from 71 CRPC metastases frozen in Optimal Cutting Temperature compound (OCT; Tissue-Tek) from 47 patients. Eight-micron–thick sections from visceral metastases ($n = 54$) were cut using a Leica CM3050S cryostat, collected on PEN Membrane Frame Slides (Life Technologies) and immediately fixed in 95% ethanol. Sections were briefly stained with hematoxylin then dehydrated in 100% ethanol. About 5,000 to 10,000 tumor cells per sample were laser capture microdissected with an Arcturus Veritas instrument and collected on CapSure Macro LCM Caps (Life Technologies). Digital photographs were taken of tissue sections before, during, and after LCM and assessed by a pathologist to confirm the tumor content. RNA was isolated using the Arcturus PicoPure RNA Isolation Kit and the samples were DNAse treated using the Qiagen RNase-Free DNase Set. RNA was amplified for two rounds using the Ambion MessageAmp aRNA Kit. The bone metastases ($n = 17$), which were frozen in OCT blocks, were sampled using 1-mm diameter tissue punch in a $-20°C$ cryostat. The sample was obtained from the region of the block where there was tumor based upon a section of an adjacent decalcified FFPE block. RNA was isolated from the tissue cores using the RNeasy Plus Micro Kit (Qiagen Inc.). Tissue cores were placed in the kit's Buffer RLT Plus, to which β-mercaptoethanol had been added, and homogenized with a disposable hard tissue homogenizer tip (Omni International). Flash-frozen LuCaP prostate cancer xenograft tissue was histologically evaluated for regions of viable tumor. RNA was isolated from 15, 10-μm sections from xenografts with $\geq$80% tumor content. For xenografts with <80% tumor, stroma and necrotic tissue were removed using an 18-guage needle before sectioning. RNA was extracted using the Qiagen RNeasy Kit, (Qiagen Inc.), according to the manufacturer's protocol. On-column DNase digestion was performed. RNA was quantified using a Nanodrop 1000 (Thermo Scientific) and quality was assessed via Agilent Bioanalyzer 2100 (Agilent Technologies).

RNA amplification and microarray hybridization

Agilent 44K whole human genome expression oligonucleotide microarrays (Agilent Technologies, Inc.) were used to profile the prostate cancer xenograft lines and CRPC metastases. Total RNA from xenograft tissue was amplified one round; patient samples were amplified two rounds as described previously (15). Probe labeling and hybridization followed Agilent protocols. Fluorescent array images were digitized using the Agilent DNA microarray scanner G2565BA. Data were less normalized within arrays (normexp background correction with offset 50) and quantile normalized between arrays in R using the Limma Bioconductor package. Control probes were removed, duplicate probes averaged, and spots flagged by Agilent Feature Extraction software as being foreground feature nonuniformity or population outliers were assigned a value of "NA." Data were normalized separately

for LuCaP xenografts and CRPC metastases. CRPC metastases were subject to an additional normalization step to remove systematic batch effects by application of the ComBat function within the sva Bioconductor package to the log2 Cy3 signal intensities (http://www.ncbi.nlm.nih.gov/geo/query/acc.cgi?token=ghylcmeynpslhel&acc=GSE66187).

Gene set enrichment analysis

Gene-expression results were ranked by their statistical analysis of microarray (SAM) *t* test score and used to conduct Gene Set Enrichment Analysis (GSEA; ref. 16) to determine patterns of pathway activation in different phenotypic groups. We used the curated pathways from the Transcription Factor database (TF) and Gene Ontology (GO) as gene sets from MSigDBv4.0.

Immunohistochemistry

Five-micron–thick sections of the TMAs were deparaffinized and rehydrated in sequential xylene and graded ethanol. Antigen retrieval was performed in 10 mmol/L citrate buffer (pH 6.0) in a pressure cooker. Endogenous peroxidase and avidin/biotin were blocked, respectively (Vector Laboratories Inc.). Sections were then incubated with 5% normal goat-horse-chicken serum, incubated with primary antibody (Supplementary Table S1), incubated with biotinylated secondary antibody (Vector Laboratories Inc.), followed by ABC reagent (Vector Laboratories Inc.), and stable DAB (Invitrogen Corp.). All sections were lightly counterstained with hematoxylin and mounted with Cytoseal XYL (Richard Allan Scientific). Mouse or rabbit IgG was used as negative controls.

Immunohistochemical assessment

Immunostaining was assessed using a quasi-continuous scoring system, created by multiplying each optical density level ("0" for no stain, "1" for faint/equivocal stain, and "2" for definitive stain) by the percentage of cells at each staining level. The sum of the three multiplicands provided a final score for each sample (score range was 0 to 200). The score for each sample was the average of the scores of each duplicate. Cytoplasm and nuclei were evaluated separately. The scores were categorized as "none" (score range: 0), "weak" (score range: 0–70), "moderate" (score range: 70–140), and "intense" (score range: 140–200). Samples with missing or damaged cores were excluded from analysis.

Western analysis

LuCaP xenografts were manually homogenized in RIPA buffer containing 2 mol/L of urea and protease inhibitors (Thermo Fisher Scientific). The homogenates were sonicated and centrifuged to remove insoluble material. Ten-micrograms of total protein lysate was electrophoresed on 4% and 12% Bis-Tris gels (Invitrogen) with MES buffer. The gels were transferred to nitrocellulose and blocked with 5% BSA in PBS/0.1% Tween-20 and subsequently probed with 1:1,000 dilution of anti-SRRM4 antibody (HPA052783; Atlas Antibodies AB) or 1:2,000 dilution of anti-GAPDH (GT239; Genetex). Protein was visualized using Supersignal West Femto Chemiluminescent Substrate (Thermo Fisher Scientific).

PCR

RNA for PCR was extracted using Stat-60 RNA isolation reagent (Tel Test Inc), according to the manufacturer's instructions. First-strand cDNA synthesis was performed with 1 μg of RNA using an Advantage RT-for-PCR Kit (Clontech Laboratories Inc.). Real-time PCR was performed using Platinum SYBR Green qPCR SuperMix-UDG (Invitrogen) on a Rotor-Gene Q (Qiagen). PCR primers (Integrated DNA Technologies) specific for *SRRM4* were designed to span an intron-exon boundary. Primers for *REST* and *SNAP25* were adapted from Raj and colleagues (11). Primers are listed in Supplementary Table S2. Four-microliters of cDNA was used per reaction with 0.2 μmol/L primers, and Platinum SYBR Green qPCR SuperMix-UDG (Invitrogen). The PCR reaction parameters were as follows: 50°C for 2 minutes and 95°C for 2 minutes (one cycle), followed by 40 cycles at 95°C for 10 seconds, annealing/extension at T(m) for 30 seconds, and 72°C for 30 seconds; the final extension was 72°C for 7 minutes. Standard curves for each amplicon were generated from a 4-fold dilution series of C4-2BE cDNA run in duplicate (all standard curves had $r > 0.99$). Reactions were carried out in duplicate, and expression levels were calculated from a standard curve. Amplicon product was confirmed by melt curve analysis. Threshold cycle of amplification (Ct) value for each gene was normalized to a housekeeping gene, *ACTB*. Fold change in mRNA expression level was calculated by the comparative C_t method using the formula $\Delta\Delta C_t$. *REST* and *REST4* PCR products were visualized after electrophoresis on a 1.2% agarose gel.

Hierarchical clustering

Genes between $CHGA^-$ versus $CHGA^+/SYP^+$ were compared and considered differentially expressed when SAM score was >3 or $\leq$3 and $P < 0.005$. The resulting 155 genes were hierarchically clustered (centroid linkage) using open source clustering software Cluster 3.0 (http://bonsai.hgc.jp/~mdehoon/software/cluster/software.htm) and the resulting heatmap was viewed using Java TreeView (http://jtreeview.sourceforge.net).

Statistical analysis

SAM program (http://www-stat.stanford.edu/~tibs/SAM/) was used to analyze expression differences between the groups. Unpaired, *t* tests were calculated for all probes passing filters and controlled for multiple testing by estimation of *q* values using the FDR method (17). Significance of differences for the IHC analyses were calculated using a Student *t* test, with *P* values $\leq$0.05 indicating statistical significance.

Results

Patient demographics, treatments, and prevalence of CRPC metastases

Patient demographics and clinical data are summarized in Supplementary Table S3. All patients received ADT; mean treatment duration was 5.6 years (range, 1.5–20.3 years). Bone, lymph nodes, and liver were the most frequent sites of metastasis.

Characterization of neuroendocrine carcinoma and adenocarcinoma with neuroendocrine differentiation in metastatic CRPC

Using a TMA of 155 CRPC metastases from 50 patients, we assessed tumor cell expression of CHGA, SYP, AR, and prostate-specific antigen (PSA; Fig. 1A). Among 50 patients, 29 patients had at least one metastasis with CHGA-stained cells and 11 patients had at least 1 metastasis with SYP stained cells. Coexpression of CHGA and SYP in the same metastasis was only

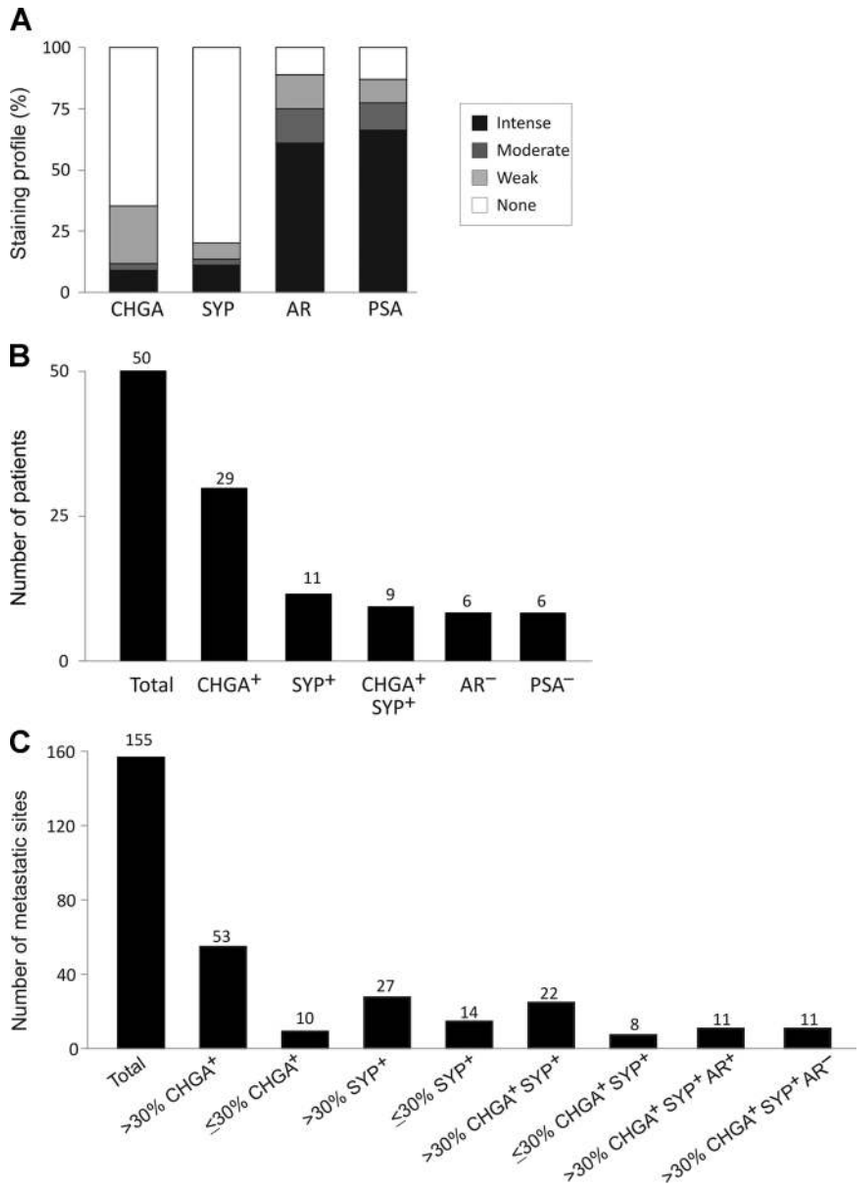

Figure 1.
IHC expression profile in CRPC metastases. A, distribution of CHGA, SYP, AR, and PSA expression in visceral and bone CRPC metastases ($n = 155$); B, the number of patients who have at least one metastasis with corresponding marker(s) expression; C, the number of metastases with corresponding marker(s) expression.

observed in 9 patients (Fig. 1B). In addition, there were 6 patients with at least 1 metastasis that expressed neither AR nor PSA (Fig. 1B). Of the 155 metastases, 63 expressed CHGA and 42 expressed SYP. Because neuroendocrine cells are normally present in most organs in small numbers, a minor population of CHGA and/or SYP-positive cells is not unexpected. To show more distinct molecular–biologic differences of those metastatic CRPC with neuroendocrine differentiation, we arbitrarily used >30% $CHGA^+$ and SYP^+ ($CHGA^+/SYP^+$) cells as a cutoff to define the CRPC sites with significant neuroendocrine differentiation. We considered a tumor with >30% $CHGA^+/SYP^+$ a significant population that could represent (i) a mixed population of neuroendocrine cells and adenocarcinoma where neuroendocrine cells were scattered throughout the tumor, or (ii) the development of a neuroendocrine derivative where all of the neuroendocrine cells were only within a specific region of the tumor.

Staining by IHC demonstrated little to no adenocarcinoma mixed with neuroendocrine carcinoma (only 1 site with >30% CHGA and SYP showed a scattered population with adenocarcinoma in this study), expression contained within a region of the tumor was more prevalent (Supplementary Fig. S1). By the criteria noted above, of 155 metastases, 53 (34%) were $CHGA^+$, 27 (17%) were SYP^+, and 22 (14%) coexpressed CHGA and SYP (Fig. 1C). The majority of metastases with a population containing >30% $CHGA^+/SYP^+$ stained with 100% positivity (Supplementary Fig. S1B and S1C).

In our study, 11 of 155 metastases (4 patients) had extensive $CHGA^+/SYP^+/AR^-$ expression. After carefully reviewing hematoxylin and eosin–stained sections, we found that these metastases histologically represented the classically defined neuroendocrine carcinoma/small cell carcinoma (Fig. 1C). In this group, cancer cells were uniformly similar to each other but dramatically

different from the conventional adenocarcinoma as illustrated by cell size, shape, nuclear-to-cytoplasmic ratio, and the lack of typical glandular structure (Supplementary Fig. S1A). All metastases that were $CHGA^+/SYP^+/AR^-$ were also PSA^-. The 11 $CHGA^+/SYP^+/AR^+$ metastases (6 patients) were morphologically indistinguishable from the surrounding adenocarcinoma, and these tumors were defined as adenocarcinoma with neuroendocrine differentiation (Supplementary Fig. S1A). All metastases that were $CHGA^+/SYP^+/AR^+$ were also PSA^+. We also determined in patients with $CHGA^+/SYP^+$ sites how many sites were not $CHGA^+/SYP^+$ (Supplementary Table S4). The molecular profiles of 71 of the 155 CRPC metastases were available for gene-expression analysis. The 71 metastases were categorized by IHC into three groups: $CHGA^-$ ($n = 51$), $CHGA^+/SYP^+$ ($n = 10$), and $CHGA^+/SYP^-$ ($n = 10$). The $CHGA^+/SYP^+$ metastases (14% total) had a distinct molecular signature when compared with the other two groups (Fig. 2).

GSEA clearly demonstrated that the $CHGA^+/SYP^+$ metastases had a neuroendocrine gene-expression signature showing enrichment of central nervous system development ($P < 0.001$), transmission of nerve impulse ($P < 0.001$), synaptic transmission ($P < 0.001$), nervous system development ($P < 0.001$), regulation of neurogenesis ($P = 0.009$), and synaptic vesicle ($P = 0.004$) in the $CHGA^+/SYP^+$ metastases. Additional GSEA comparison of metastases displaying the classic $CHGA^+/SYP^+/AR^-$ neuroendocrine phenotype versus $CHGA^+/SYP^-$ and $CHGA^-$ metastases using Gene Ontology (GO) terms showed enrichment of central nervous system development ($P < 0.001$), transmission of nerve impulse ($P < 0.001$), synaptic transmission ($P < 0.001$), nervous system development ($P < 0.001$), regulation of neurogenesis ($P = 0.01$), and synaptic vesicle ($P = 0.038$) in the $CHGA^+/SYP^+/AR^-$ metastases. In addition, notably the transcription factor (TF) database revealed that genes with promoter regions [−2kb,2kb] around transcription start sites containing REST, were the most differentially enriched between the $CHGA^+/SYP^+/AR^-$ metastases and all other metastases ($P < 0.001$). Comparing $CHGA^+/SYP^+/AR^+$ versus $CHGA^-$ and $CHGA^+/SYP^-$ metastases in GO, neuronal gene sets were enriched in the $CHGA^+/SYP^+/AR^+$ metastases, including but not limited to nervous system development ($P < 0.001$), synaptic vesicle ($P = 0.029$), neuron development ($P = 0.038$), neuron differentiation ($P = 0.024$), and neurogenesis ($P = 0.008$). Results of a TF database search showed that the most differentially expressed genes were enriched for the REST-binding motif in their promoter regions ($P < 0.001$). Genes defining this subpopulation of metastases cluster into a defined $CHGA^+/SYP^+$ group (Supplementary Fig. S2). This led us

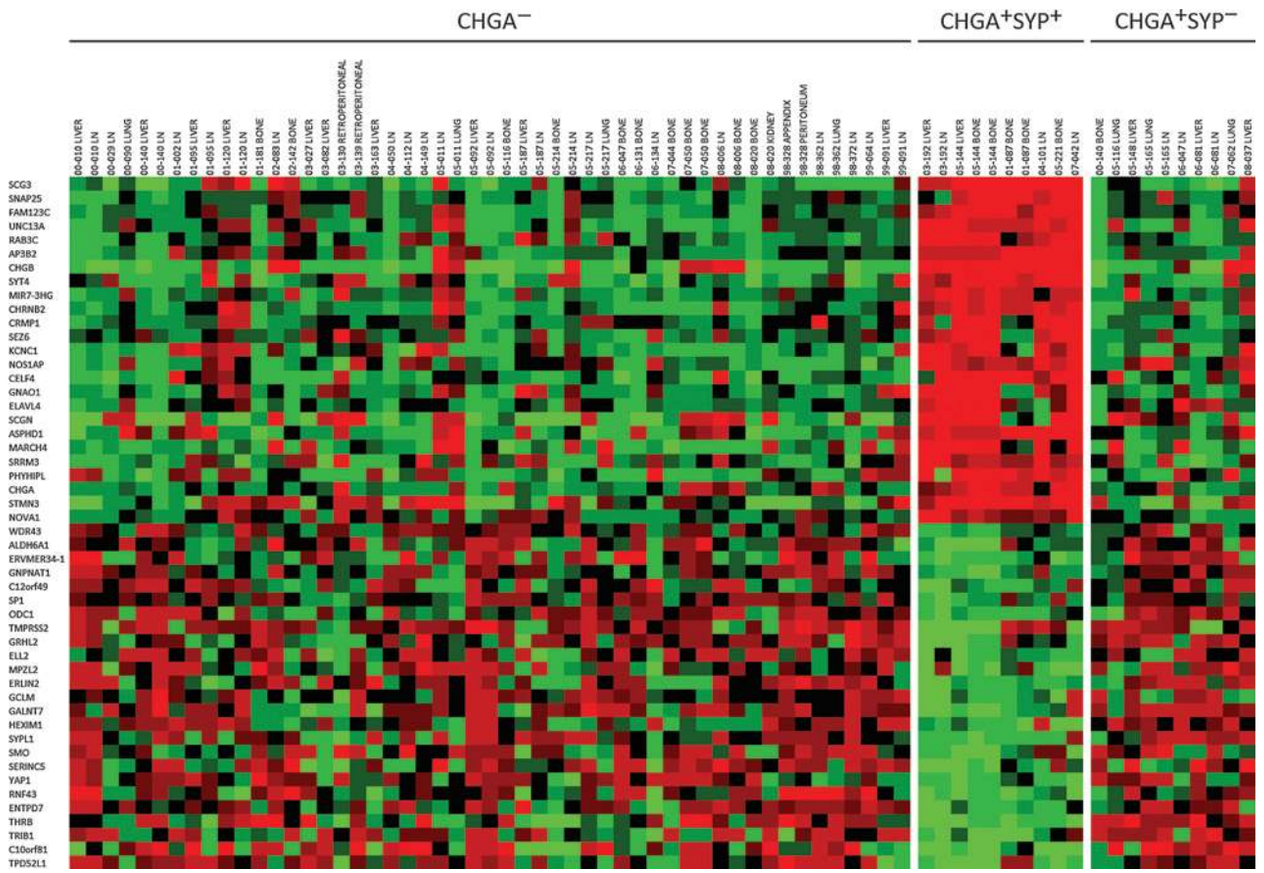

Figure 2.
Agilent oligo array expression analysis of the top and bottom 25 neuroendocrine/neuronal-associated genes in CRPC metastases. Categories ($CHGA^-$, $CHGA^+/SYP^+$, $CHGA^+/SYP^-$) are based on the IHC results for CHGA and SYP on paraffin-embedded tissue from the same metastases. Mean-centered ratios of genes are colored according to scale (Supplementary Fig. S2).

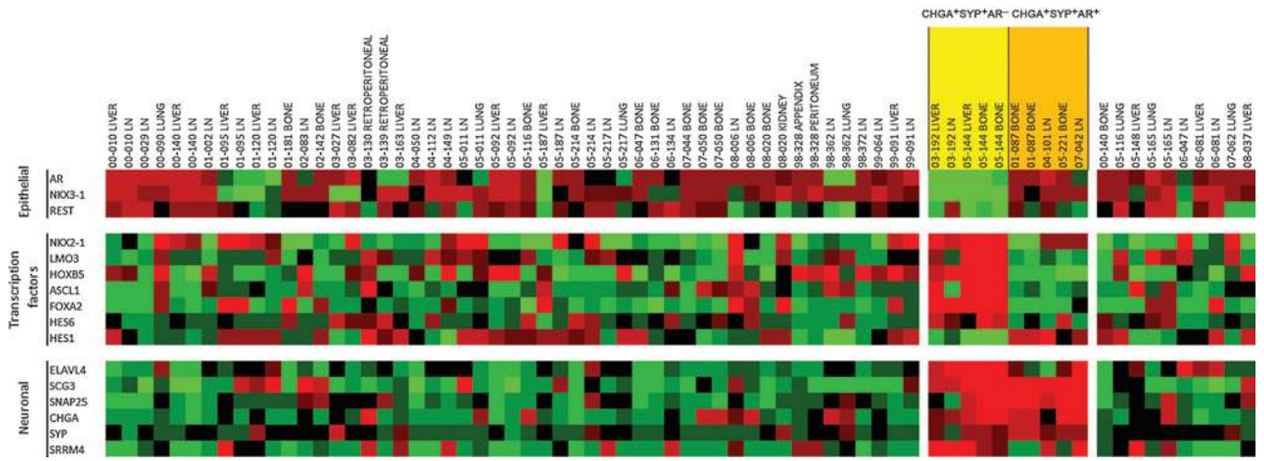

Figure 3.

Agilent oligo array expression analysis of relevant prostate epithelial, transcription factor, and neuroendocrine/neuronal-associated genes that differentiate neuronal AR^+ and AR^- metastases in CRPC. Neuroendocrine tumors are highlighted in orange (AR^+) and yellow (AR^-). Mean-centered ratios of genes are colored according to scale (Supplementary Fig. S2).

to conclude that the CRPC neuroendocrine molecular phenotype defined by $CHGA^+/SYP^+$ dual positivity as detected by IHC, is more common in CRPC than historically noted in hormone sensitive primary disease (7), and that $CHGA^+/SYP^+/AR^-$ metastases expressed additional neuronal-associated genes when compared with $CHGA^+/SYP^+/AR^+$ metastases.

The neuroendocrine molecular profile in CRPC metastases is mitigated by AR expression

From 10 $CHGA^+/SYP^+$ metastases, 5 metastases from 4 patients were AR^+ and 5 metastases from 2 patients were AR^-. To further define the molecular profile of the $CHGA^+/SYP^+$ metastases, we compared the gene-expression profiles of the 10 $CHGA^+/SYP^+/AR^+$ and $CHGA^+/SYP^+/AR^-$ metastases. We focused on prostate epithelial-associated transcriptional regulators, known neuroendocrine transcription factors and regulators, and downstream neuroendocrine associated genes (Fig. 3). $CHGA^+/SYP^+/AR^+$ metastases expressed *NKX3.1* and *REST*. $CHGA^+/SYP^+/AR^-$ metastases had a decrease in *NKX3.1* with one patient, exhibiting a decrease in *REST* expression and the other patient displaying no change in *REST* expression relative to adenocarcinoma (Fig. 3). A number of other transcription factors have been associated with neuroendocrine gene expression (*NKX2.1*, *LMO3*, *HOXB5*, *FOXA2*, *HES6*, *HES1*, and *ASCL1*; refs. 18–26) (Supplementary Fig. S3A). We observed an increase in all of these transcription factors (except *HES1*, which as expected decreased) in the $CHGA^+/SYP^+/AR^-$ metastases relative to the $CHGA^+/SYP^+/AR^+$ metastases. This suggests that these neuroendocrine-associated transcription factors are repressed in the AR expressing cells. However, the expression of downstream well-known neuroendocrine genes, including but not limited to *ELAVL4*, *SCG3*, *SNAP25*, *CHGA*, *SYP*, and *SRRM4*, was increased in both $CHGA^+/SYP^+/AR^-$ and $CHGA^+/SYP^+/AR^+$ metastases relative to the $CHGA^-$ and $CHGA^+/SYP^-$ metastases. These data imply that there are two phenotypes within the $CHGA^+/SYP^+$ metastases. A Venn diagram comparing genes with SAM score >2.5 in $CHGA^+/SYP^+/AR^+$ metastases and $CHGA^+/SYP^+/AR^-$ metastases versus $CHGA^+/SYP^-$ and $CHGA^-$ metastases, respectively, shows that the latter displayed more differentially expressed genes (598 vs. 61). Thirty-seven genes were common to all $CHGA^+/SYP^+$ metastases with SAM score >2.5 relative to the $CHGA^-$ and $CHGA^+/SYP^-$ metastases (Supplementary Fig. S3B). Notably, these genes included *SRRM4* and *SNAP25*, which is directly repressed by REST (Supplementary Fig. S4; ref. 11).

Expression of NKX-homeodomain factors is altered with neuroendocrine differentiation in CRPC

Thyroid transcription factor 1 (TTF-1), the gene product of *NKX2-1*, was significantly higher as detected by IHC in $CHGA^+/SYP^+/AR^-$ metastases compared with $CHGA^-$ or $CHGA^+/SYP^-$ metastases ($P < 0.001$). TTF-1 was not significantly different in $CHGA^+/SYP^+/AR^+$ metastases compared to $CHGA^-$ or $CHGA^+/SYP^-$ metastases (Fig. 4A). NKX3-1 protein nuclear localization was completely lost in $CHGA^+/SYP^+/AR^-$ metastases ($P < 0.001$), whereas maintained in $CHGA^+/SYP^+/AR^+$ metastases (Fig. 4B).

Secretogranin III (SCG3) as a potential neuroendocrine marker

Our analyses showed that *SCG3* was the most upregulated gene in $CHGA^+/SYP^+$ metastases relative to all other metastases (Fig. 2). SCG3 protein was also significantly higher by IHC relative to $CHGA^-$ and $CHGA^+/SYP^-$ metastases ($P<0.001$) (Fig. 4C). Although highly expressed in both, SCG3 was higher in the $CHGA^+/SYP^+/AR^-$ neuroendocrine metastases relative to the $CHGA^+/SYP^+/AR^+$ metastases ($P<0.01$). SCG3 immunoreactivity was cytoplasmic with various staining patterns, including sporadic intensely stained single cells, an apocrine pattern with positively stained cytoplasmic membrane-bound vesicles budding in the lumen, a mixture of apocrine pattern with cytoplasmic positivity, and a homogeneous cytoplasmic staining pattern (Fig. 4C; a through d).

HuD expression is determined by AR expression in neuroendocrine CRPC metastases

HuD (*ELAVL4*) was stained in 22.4% of all metastatic CRPC in the nucleus and/or cytoplasm. $CHGA^+/SYP^+/AR^-$ metastases had the highest protein level among the three subgroups ($P < 0.001$),

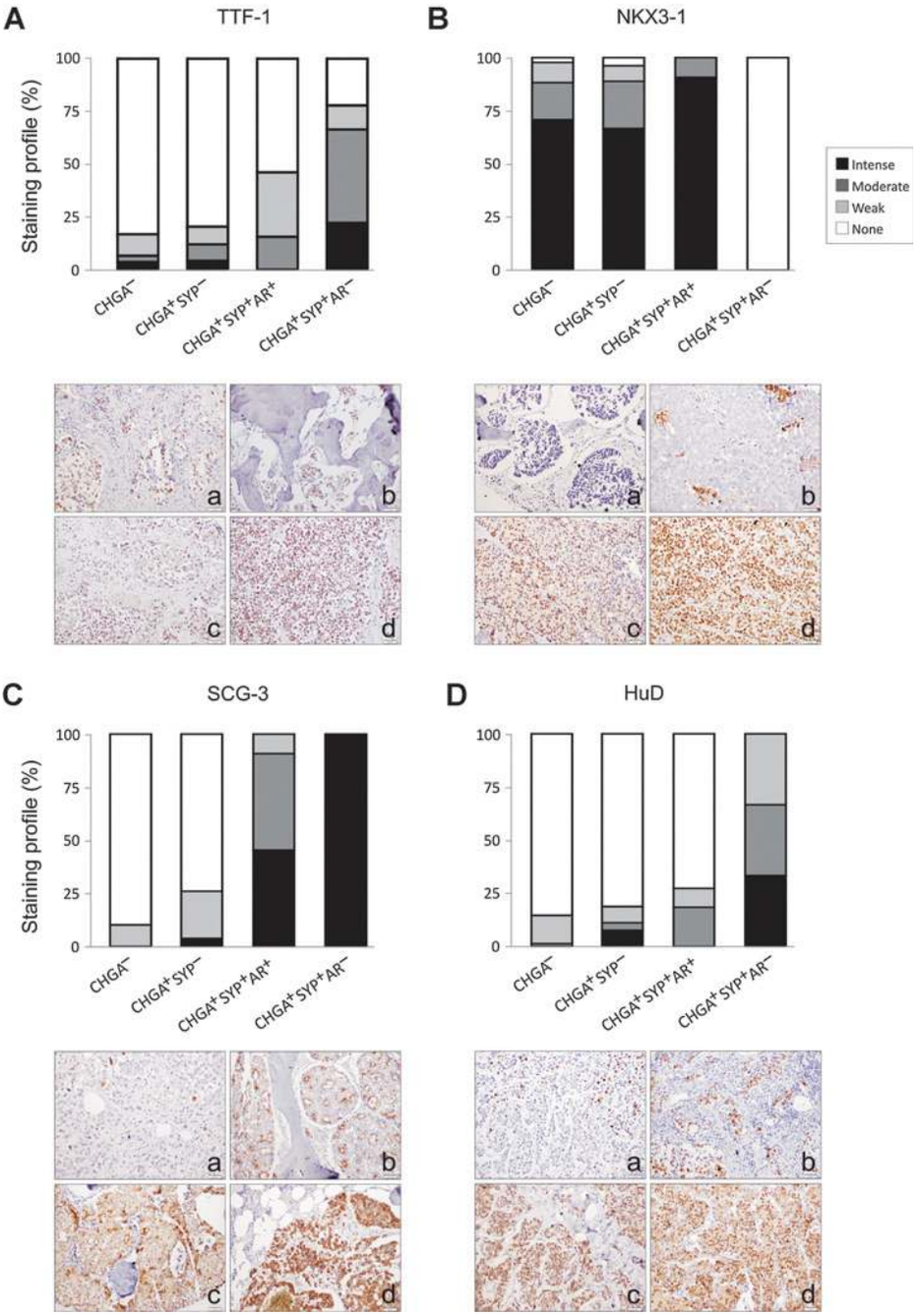

Figure 4.
IHC analysis of TTF-1 (A), NKX3.1 (B), SCG3 (C), and HuD (D) in CRPC metastases ($n = 155$). We observed increased expression of TTF-1 in neuroendocrine CRPC, a loss of NKX3.1 expression in AR^- neuroendocrine CRPC, increased expression of SCG3 in neuroendocrine CRPC, and an increase in expression of HuD in AR^- neuroendocrine CRPC. The difference in the expression of each of these proteins underlines the biology associated with AR^+ and AR^- neuronal phenotype in CRPC metastases. Representative pictures of stained metastases are shown. TTF-1 and NKX3-1 staining was mainly nuclear (A, a–d) and (B, a–d), respectively. SCG3 was cytoplasmic with various staining patterns: sporadic intensely stained single cells (C, a); an apocrine pattern, with positive stained cytoplasmic membrane-bound vesicles budding in the lumen (C, b); a mixture of apocrine pattern with cytoplasmic positivity (C, c); and a homogeneous cytoplasmic staining pattern (C, d). HuD staining was mainly nuclear (D, a–d).

suggesting that it is preferentially expressed by $CHGA^+/SYP^+$ tumors when AR is absent (Fig. 4D).

Gene-expression analysis of AR-negative neuroendocrine LuCaP PDX models reveals a signature similar to that of AR-negative neuroendocrine metastases from patients

We used four neuroendocrine AR-negative neuroendocrine LuCaP PDXs for our analyses. LuCaP 49 (27), LuCaP 93, LuCaP 145.1, and LuCaP 145.2. The gene-expression profiles of these neuroendocrine PDX models were compared with 20 LuCaP adenocarcinoma PDX models. All neuroendocrine LuCaP xenografts were AR^- (Supplementary Figs. SS6 and SS7). Gene-expression analysis looking at *NKX3-1* and *REST* reveal results concordant with the results in the CRPC $CHGA^+/SYP^+/AR^-$ metastases (Fig. 5). *NKX2-1*, *LMO3*, *HOXB5*, *ASCL1*, *FOXA2*, *HES6*, *HES1*, *ELAVL4*, *SCG3*, *SNAP25*, *CHGA*, *SYP*, and *SRRM4* all had a similar pattern of expression to the CRPC $CHGA^+/SYP^+/AR^-$ metastases (Fig. 5). It is important to note that LuCaP 145.1 and 145.2 were derived from two different metastases from patient 05-144 on the gene-expression array.

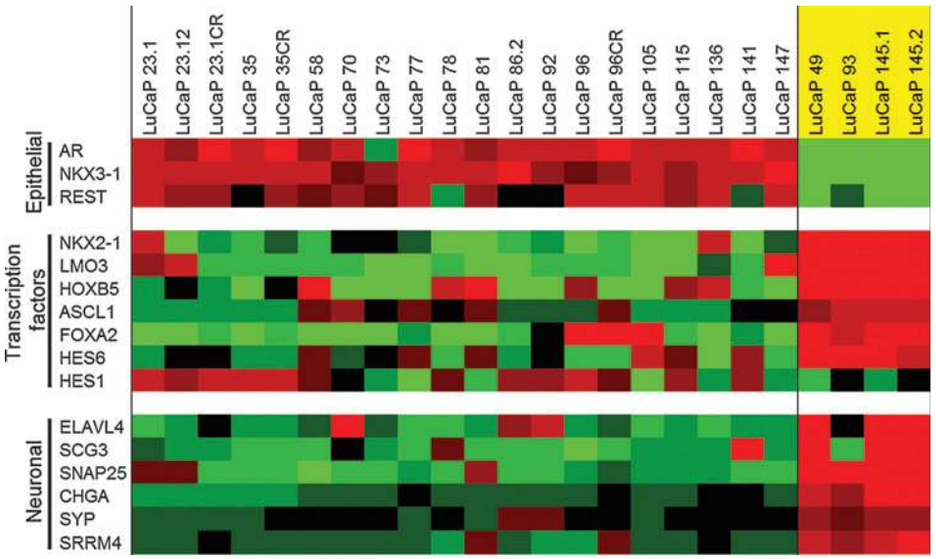

Figure 5.
Agilent oligo array expression analysis of relevant prostate epithelial, transcription factor, and neuroendocrine/neuronal-associated genes that differentiate neuronal LuCaP xenografts. AR^- neuroendocrine xenografts are highlighted in yellow. Mean-centered ratios of genes are colored according to scale (Supplementary Fig. S2).

IHC of proteins identified by gene-expression analysis in AR-negative neuroendocrine LuCaP PDX models

The 4 neuroendocrine LuCaP PDX models share common biologic features, including expression of CHGA (only observed in this study by gene-expression analysis in LuCaP 49), SYP, and downregulation of AR and PSA (Supplementary Fig. S6A and S6B). TTF-1, NKX3-1, SCG3, and HuD expressions at the transcript and protein levels were similar to those observed in $CHGA^+/SYP^+/AR^-$ metastases (Supplementary Fig. S6A).

SRRM4 is expressed and may promote the neuroendocrine phenotype in neuroendocrine metastatic tissues and neuroendocrine LuCaP PDX models

SRRM4 promotes alternative splicing and inclusion of neural-specific exons (11, 28). We identified *SRRM4* as a gene expressed in neuroendocrine patient tissues and LuCaP PDX models (Figs. 4 and 6). SRRM4 splices a 62bp exon into *REST* (11). Using PCR primers designed to identify the splicing-in event between exon 3 and 4 in the REST mRNA, we observed two bands, one at approximately 124 bp and another at approximately 186 bp in 2 AR-negative and 2 AR-positive patients with a neuroendocrine phenotype (Fig. 6A). Suggesting that the splicing of REST occurs in neuroendocrine metastases. We then went on to determine whether this event could also be observed in the neuroendocrine LuCaP PDX models. Western blot analysis showed that SRRM4 was upregulated in all four neuroendocrine LuCaP PDX models when compared with four randomly selected adenocarcinoma LuCaP PDX models (Fig. 6B). As mentioned previously for the neuroendocrine patient metastases, using PCR primers designed to identify the splicing-in event between exon 3 and 4 in the REST mRNA, we observed two bands, one at approximately 124 bp and another at approximately 186 bp in all four neuroendocrine LuCaP models. Only one 124 bp band was observed in the 4 adenocarcinoma LuCaP models (Fig. 6C), suggesting that 62 bp's were inserted into *REST* producing *REST4* in the LuCaP neuroendocrine xenografts. The same samples were used to determine *SRRM4*, *REST*, and *SNAP25* expression by qPCR (Fig. 6D). The average $\Delta\Delta C_t$ was −3.5 for total *REST*, 7.4 for *SRRM4*, and 11.3 for *SNAP25* in LuCaP neuroendocrine xenografts versus LuCaP adenocarcinoma. The increase in SRRM4 expression, splicing in of 62 bp into *REST*, the loss of *REST* expression, and increase in *SNAP25* expression imply that SRRM4 is promoting the neuroendocrine phenotype in LuCaP neuroendocrine xenografts.

Discussion

It has been proposed that prostate adenocarcinoma cells are able to "transdifferentiate" into neuroendocrine cells under certain pathologic circumstances, including ADT. The transdifferentiating cells acquire the ability to express neuroendocrine-associated proteins whereas some of these cells still maintain epithelial characteristics (9). The neuroendocrine cells in CRPC most likely have multiple origins, morphologies, and molecular phenotypes (29–32). In our study, we identified patients and metastases that have neuroendocrine features based on IHC analysis and associated gene-expression signatures. There is suggestive evidence from our study that support the hypothesis that neuroendocrine tumors can develop from adenocarcinoma in response to ADT: (i) the greater number of patients with neuroendocrine disease in CRPC relative to hormone naïve patients, (ii) the presence of metastases with adenocarcinoma and other metastases with neuroendocrine features in the same patient, (iii) the presence of metastases with a mix of cells with both adenocarcinoma and neuroendocrine features at the same site, and (iv) the presence of metastases with neuroendocrine features that are AR^+.

This study highlights the findings that the use of a limited number of biomarkers to define the neuroendocrine phenotype in CRPC could be somewhat misleading. For example, if CHGA was the only marker used to define neuroendocrine cells, our data would suggest that up to a third of all of the metastases in our cohort would be considered to be neuroendocrine metastases. In addition, it appears that rather than transforming into the neuroendocrine phenotype based on CHGA and SYP positivity, neuroendocrine AR^+ cells can take on the appearance of a neuroendocrine cell while retaining aspects of their original lineage. On the basis of our detailed analysis of clinical specimens and PDX models, the coexpression of SYP is required before a metastasis has a discernable neuroendocrine molecular phenotype with

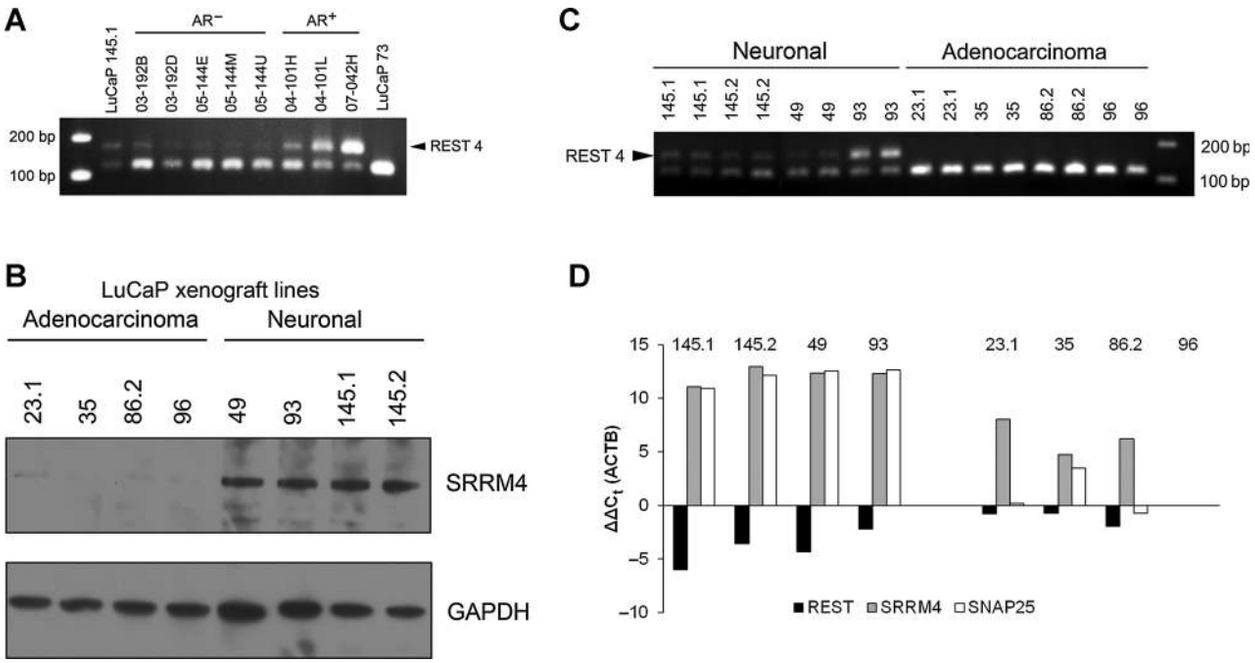

Figure 6.

SRRM4 expression and REST splicing in patient metastases and LuCaP xenografts. A, PCR demonstrating *REST* is spliced inserting a 62-bp exon producing *REST4* (indicated by arrow) in AR^- and AR^+ metastatic sites from each of four patients. LuCaP 145.1 (neuroendocrine and splicing control); LuCaP 73 (adenocarcinoma and no splicing control). B, Western analysis of SRRM4 in adenocarcinoma and neuronal xenografts, (C) PCR demonstrating *REST* is spliced producing *REST4* (indicated by arrow) in the four neuronal LuCaP PDX lines, and (D) qPCR of *REST*, *SRRM4*, and *SNAP25* (a gene repressed by REST) expression with actin as a reference in neuronal and adenocarcinoma LuCaP PDX lines. Transcript levels are defined relative to LuCaP 96 (an adenocarcinoma).

the loss of AR expression leading to a more succinct neuroendocrine phenotype. Our study highlights the fact that only $CHGA^+/SYP^+/AR^-$ CRPC metastases had a molecular signature associated with the neuroendocrine phenotype, whereas $CHGA^+/SYP^+/AR^+$ metastases had a signature associated with the loss of REST activity. Our analyses also provide additional biomarkers that may further distinguish the neuroendocrine phenotype in CRPC (Supplementary Fig. S5).

As stated previously, our analysis identified $CHGA^+/SYP^+/AR^+$ cells having aspects of both a neuroendocrine and an adenocarcinoma phenotype, expressing genes that are associated with a neuroendocrine phenotype and genes downstream of the AR. Furthermore, the identification of $CHGA^+/SYP^+/AR^+$ cells with apocrine expression of secreted proteins (e.g. SCG3) suggests that the cells are retaining a polarized secretory phenotype, while secreting neuroendocrine secretory products in addition to PSA, etc. We hypothesize that the expression of active SRRM4 could be sufficient to promote this phenotype by blocking the activity of REST. This raises the question: Is the $CHGA^+/SYP^+/AR^+$ phenotype a sheep in wolfs' clothing, that is, because genes downstream of the AR are present in these cells, it is possible that these cells will still respond to ADT? This still remains to be elucidated.

On the basis of the GSEA, similar to the $CHGA^+/SYP^+/AR^+$ phenotype, the $CHGA^+/SYP^+/AR^-$ phenotype–expressed genes are usually repressed by REST. However, a considerable number of additional transcription factors and downstream genes were transcribed in the AR^- phenotype. This indicates that these tumors will not respond to ADT and further suggests that these tumors have a more neuroendocrine-like phenotype.

With the advent of total androgen blockade for the treatment of metastatic prostate cancer, the suggestion has been made that there could be a significant increase in the number of patients with neuroendocrine disease (32). The biospecimens used from 50 patients in our study were from 1998 to 2008. Even during this time period with the limited repertoire of primary and secondary hormonal treatments, we see the emergence of the neuroendocrine phenotype in these patients. Whether longer and more aggressive hormonal therapy will lead to a greater propensity for the evolution of neuroendocrine tumors from adenocarcinoma with a greater proportion of neuroendocrine metastases in a patient remains to be seen. However, it should be recognized that some patients who have metastases with the $CHGA^+/SYP^+/AR^+$ phenotype may still respond to ADT. Moreover, although a patient may have a population of $CHGA^+/SYP^+/AR^-$ metastasis, it cannot be assumed that all metastases in that patient are $CHGA^+/SYP^+/AR^-$.

It has been suggested for some time that REST plays a role in the emergence of the neuroendocrine phenotype in CRPC. However, although the loss of REST has been associated with the loss of AR activity, hypoxia, and IL6 expression (33–35), this was not always evident in our sample-set given the continued expression of REST in some neuroendocrine tumors (36). SRRM4 promotes alternative splicing and inclusion of neural-specific exons (11). We have shown that the expression of SRRM4 is associated with the neuroendocrine phenotype in CRPC metastases, and that the splicing of REST occurs in our AR^- neuroendocrine PDX models. The splicing in of 62 bp into REST mRNA thereby inactivating REST could explain our results, but it does not preclude the fact that in some cases the loss of REST activity alone (through

repression, methylation, mutation, genomic rearrangement, or loss), rather than the expression of SRRM4 in CRPC could result in development of the neuroendocrine phenotype.

We are aware of limitations to our study, including small sample size and a lack of functional data, to show that SRRM4 can drive CHGA and SYP expression in CRPC metastases. In addition, based on our analyses, we cannot make any conclusions as to why there is a loss of AR in some $CHGA^+/SYP^+$ metastases and not others. Finally, we arbitrarily classified tumors as neuroendocrine if the metastasis had >30% CHGA- and SYP-positive cells. It has been suggested that the presence of neuroendocrine cells can affect tumor biology and outcomes (37). Therefore, it is possible that in those metastases where neuroendocrine cells were present, but the percentage of cells was <30%, secretion of neuroendocrine factors into the microenvironment could influence the behavior of the cells with an adenocarcinoma phenotype.

In conclusion, we hypothesize that the evolution of adenocarcinoma from a hormone-sensitive state to a castration-resistant neuroendocrine phenotype is associated with the loss of REST or of REST-repressor activity due to alternate splicing by SRRM4. Yet unknown, is whether AR^+ neuroendocrine metastases will respond to new androgen deprivation therapies and what triggers the loss of AR expression in neuroendocrine tumors.

Disclosure of Potential Conflicts of Interest

L.D. True reports receiving commercial research grants from Ventana/Roche. C.S. Higano has ownership interest (including patents) in CTI Biopharma; is a consultant/advisory board member for Aragon Pharmaceuticals, Astellas Pharma Inc., Bayer Corporation, Dendreon, Genentech, Millennium Pharmaceuticals, Orion, Pfizer Inc., and Sotio/Chiltern; and reports receiving commercial research grants from Algeta ASA, Aragon Pharmaceuticals, Inc., AstraZeneca AB, Bayer HealthCare, Dendreon, Emergent BioSolutions, Genentech, Medivation, Millennium Pharmaceuticals, and Sanofi U.S. Services Inc. No potential conflicts of interest were disclosed by the other authors.

Authors' Contributions

Conception and design: X. Zhang, B. Montgomery, P.H. Lange, P.S. Nelson, C. Morrissey

Development of methodology: X. Zhang, L.G. Brown, L.D. True, J.M. Lucas, R. Dumpit

Acquisition of data (provided animals, acquired and managed patients, provided facilities, etc.): X. Zhang, L.G. Brown, L. Kollath, J.M. Lucas, R. Dumpit, E. Corey, L. Chéry, C.S. Higano, B. Montgomery, M. Roudier, R.L. Vessella, C. Morrissey

Analysis and interpretation of data (e.g., statistical analysis, biostatistics, computational analysis): X. Zhang, I.M. Coleman, L.G. Brown, L.D. True, L. Kollath, J.M. Lucas, H.-M. Lam, P.S. Nelson, C. Morrissey

Writing, review, and/or revision of the manuscript: X. Zhang, I.M. Coleman, L.D. True, L. Kollath, J.M. Lucas, H.-M. Lam, R. Dumpit, E. Corey, B. Lakely, C.S. Higano, B. Montgomery, P.H. Lange, P.S. Nelson, R.L. Vessella, C. Morrissey

Administrative, technical, or material support (i.e., reporting or organizing data, constructing databases): L.G. Brown, E. Corey, B. Lakely, P.H. Lange, R.L. Vessella, C. Morrissey

Study supervision: P.H. Lange, C. Morrissey

Acknowledgments

The authors thank the patients and their families for participating in the Prostate Cancer Donor Program, without whom this research would not have been possible. The authors also thank Khanhthy Doan, Jennifer Noteboom, Roger Coleman, Belinda Nghiem, Funda Vakar-Lopez, Beatrice Knudsen, Evan Yu, Elahe Mostaghel, Heather Cheng, and the rapid autopsy teams in the Urology Department at the University of Washington.

Grant Support

This work was supported by resources from the VA Puget Sound Health Care System, Seattle, Washington (R.L. Vessella is a research career scientist, P.H. Lange is a staff physician), the Institute for Prostate Cancer Research, the Pacific Northwest Prostate Cancer SPORE (P50CA97186), an NIH grant (PO1CA085859), the Richard M. Lucas Foundation, and the Prostate Cancer Foundation. C. Morrissey is a recipient of a Career Development Award from Jim and Cathrine Allchin.

The costs of publication of this article were defrayed in part by the payment of page charges. This article must therefore be hereby marked *advertisement* in accordance with 18 U.S.C. Section 1734 solely to indicate this fact.

Received March 14, 2015; revised April 29, 2015; accepted May 14, 2015; published OnlineFirst June 12, 2015.

References

1. Aprikian AG, Cordon-Cardo C, Fair WR, Reuter VE. Characterization of neuroendocrine differentiation in human benign prostate and prostatic adenocarcinoma. Cancer 1993;71:3952–65.
2. Vashchenko N, Abrahamsson PA. Neuroendocrine differentiation in prostate cancer: implications for new treatment modalities. Eur Urol 2005;47:147–55.
3. Abrahamsson PA. Neuroendocrine cells in tumour growth of the prostate. Endocr Relat Cancer 1999;6:503–19.
4. di Sant'Agnese PA. Neuroendocrine cells of the prostate and neuroendocrine differentiation in prostatic carcinoma: a review of morphologic aspects. Urology 1998;51:121–4.
5. Komiya A, Yasuda K, Watanabe A, Fujiuchi Y, Tsuzuki T, Fuse H. The prognostic significance of loss of the androgen receptor and neuroendocrine differentiation in prostate biopsy specimens among castration-resistant prostate cancer patients. Mol Clin Oncol 2013;1:257–62.
6. McWilliam LJ, Manson C, George NJ. Neuroendocrine differentiation and prognosis in prostatic adenocarcinoma. Br J Urol 1997;80:287–90.
7. di Sant'Agnese PA, Cockett AT. Neuroendocrine differentiation in prostatic malignancy. Cancer 1996;78:357–61.
8. Aprikian AG, Cordon-Cardo C, Fair WR, Zhang ZF, Bazinet M, Hamdy SM, et al. Neuroendocrine differentiation in metastatic prostatic adenocarcinoma. J Urol 1994;151:914–9.
9. Perrot V. Neuroendocrine differentiation in the progression of prostate cancer: an update on recent developments. Open J Urol 2012;2:173–82.
10. Nelson EC, Cambio AJ, Yang JC, Ok JH, Lara PN Jr, Evans CP. Clinical implications of neuroendocrine differentiation in prostate cancer. Prostate Cancer Prostatic Dis 2007;10:6–14.
11. Raj B, O'Hanlon D, Vessey JP, Pan Q, Ray D, Buckley NJ, et al. Cross-regulation between an alternative splicing activator and a transcription repressor controls neurogenesis. Mol Cell 2011;43:843–50.
12. Bruce AW, Donaldson IJ, Wood IC, Yerbury SA, Sadowski MI, Chapman M, et al. Genome-wide analysis of repressor element 1 silencing transcription factor/neuron-restrictive silencing factor (REST/NRSF) target genes. Proc Natl Acad Sci U S A 2004;101:10458–63.
13. Morrissey C, Roudier MP, Dowell A, True LD, Ketchanji M, Welty C, et al. Effects of androgen deprivation therapy and bisphosphonate treatment on bone in patients with metastatic castration-resistant prostate cancer: results from the University of Washington Rapid Autopsy Series. J Bone Miner Res 2013;28:333–40.
14. Corey E, Quinn JE, Buhler KR, Nelson PS, Macoska JA, True LD, et al. LuCaP 35: a new model of prostate cancer progression to androgen independence. Prostate 2003;55:239–46.
15. Sharma A, Yeow WS, Ertel A, Coleman I, Clegg N, Thangavel C, et al. The retinoblastoma tumor suppressor controls androgen signaling and human prostate cancer progression. J Clin Invest 2010;120:4478–92.
16. Subramanian A, Tamayo P, Mootha VK, Mukherjee S, Ebert BL, Gillette MA, et al. Gene set enrichment analysis: a knowledge-based approach for

interpreting genome-wide expression profiles. Proc Natl Acad Sci U S A 2005;102:15545–50.
17. Tusher VG, Tibshirani R, Chu G. Significance analysis of microarrays applied to the ionizing radiation response. Proc Natl Acad Sci U S A 2001;98:5116–21.
18. Goulburn AL, Alden D, Davis RP, Micallef SJ, Ng ES, Yu QC, et al. A targeted NKX2.1 human embryonic stem cell reporter line enables identification of human basal forebrain derivatives. Stem Cells 2011;29:462–73.
19. Isogai E, Ohira M, Ozaki T, Oba S, Nakamura Y, Nakagawara A. Oncogenic LMO3 collaborates with HEN2 to enhance neuroblastoma cell growth through transactivation of Mash1. PLoS ONE 2011;6:e19297.
20. Zhu J, Garcia-Barcelo MM, Tam PK, Lui VC. HOXB5 cooperates with NKX2-1 in the transcription of human RET. PLoS ONE 2011;6:e20815.
21. Clegg N, Ferguson C, True LD, Arnold H, Moorman A, Quinn JE, et al. Molecular characterization of prostatic small-cell neuroendocrine carcinoma. Prostate 2003;55:55–64.
22. Ball DW. Achaete-scute homolog-1 and Notch in lung neuroendocrine development and cancer. Cancer Lett 2004;204:159–69.
23. Gupta A, Yu X, Case T, Paul M, Shen MM, Kaestner KH, et al. Mash1 expression is induced in neuroendocrine prostate cancer upon the loss of Foxa2. Prostate 2013;73:582–9.
24. Mirosevich J, Gao N, Gupta A, Shappell SB, Jove R, Matusik RJ. Expression and role of Foxa proteins in prostate cancer. Prostate 2006; 66:1013–28.
25. Hu Y, Wang T, Stormo GD, Gordon JI. RNA interference of achaete-scute homolog 1 in mouse prostate neuroendocrine cells reveals its gene targets and DNA binding sites. Proc Natl Acad Sci U S A 2004;101: 5559–64.
26. Somasundaram K, Reddy SP, Vinnakota K, Britto R, Subbarayan M, Nambiar S, et al. Upregulation of ASCL1 and inhibition of Notch signaling pathway characterize progressive astrocytoma. Oncogene 2005;24:7073–83.
27. True LD, Buhler K, Quinn J, Williams E, Nelson PS, Clegg N, et al. A neuroendocrine/small cell prostate carcinoma xenograft-LuCaP 49. Am J Pathol 2002;161:705–15.
28. Calarco JA, Superina S, O'Hanlon D, Gabut M, Raj B, Pan Q, et al. Regulation of vertebrate nervous system alternative splicing and development by an SR-related protein. Cell 2009;138:898–910.
29. Epstein JI, Amin MB, Beltran H, Lotan TL, Mosquera JM, Reuter VE, et al. Proposed morphologic classification of prostate cancer with neuroendocrine differentiation. Am J Surg Pathol 2014;38:756–67.
30. Zhang T, Armstrong AJ. Clinical phenotypes of castration-resistant prostate cancer. Clin Adv Hematol Oncol 2013;11:707–18.
31. Terry S, Beltran H. The many faces of neuroendocrine differentiation in prostate cancer progression. Front Oncol 2014;4:60.
32. Beltran H, Tomlins S, Aparicio A, Arora V, Rickman D, Ayala G, et al. Aggressive variants of castration-resistant prostate cancer. Clin Cancer Res 2014;20:2846–50.
33. Svensson C, Ceder J, Iglesias-Gato D, Chuan YC, Pang ST, Bjartell A, et al. REST mediates androgen receptor actions on gene repression and predicts early recurrence of prostate cancer. Nucleic Acids Res 2014;42:999–1015.
34. Liang H, Studach L, Hullinger RL, Xie J, Andrisani OM. Down-regulation of RE-1 silencing transcription factor (REST) in advanced prostate cancer by hypoxia-induced miR-106b∼25. Exp Cell Res 2014;320:188–99.
35. Zhu Y, Liu C, Cui Y, Nadiminty N, Lou W, Gao AC. Interleukin-6 induces neuroendocrine differentiation (NED) through suppression of RE-1 silencing transcription factor (REST). Prostate 2014;74:1086–94.
36. Lapuk AV, Wu C, Wyatt AW, McPherson A, McConeghy BJ, Brahmbhatt S, et al. From sequence to molecular pathology, and a mechanism driving the neuroendocrine phenotype in prostate cancer. J Pathol 2012;227:286–97.
37. Krauss DJ, Hayek S, Amin M, Ye H, Kestin LL, Zadora S, et al. Prognostic significance of neuroendocrine differentiation in patients with Gleason score 8–10 prostate cancer treated with primary radiotherapy. Int J Radiat Oncol Biol Phys 2011;81:e119-e125.